THE AMERICAN SOCIETY OF MECHANICAL ENGINEERS
Three Park Avenue, New York, N.Y. 10016-5990

99-GT-384



# TRANSONIC COMPRESSOR INFLUENCES ON UPSTREAM SURFACE PRESSURES WITH AXIAL SPACING

Peter J. Koch, Douglas P. Probasco and J. Mitch Wolff
Department of Mechanical & Materials Engineering
Wright State University
Dayton, OH

William W. Copenhaver
Air Force Research Laboratory
Wright-Patterson Air Force Base, OH

Randall M. Chriss
NASA Lewis Research Center
Cleveland, OH



## ABSTRACT

A set of inlet guide vane (IGV) unsteady surface pressure measurements is presented. The unsteady aerodynamic effects of a highly loaded, high speed downstream compression stage on the upstream inlet guide vane stator surface pressures are characterized through experimental and computational analysis. The axial spacing between the IGV and rotor was varied between 12%, 26%, and 56% of the IGV chord for a 105% speed, peak efficiency operating condition, which is transonic. Unsteady IGV surface pressures were acquired for two spanwise locations on both blade surfaces. The largest unsteady surface pressure magnitudes were obtained at the 12% axial spacing configuration and 95% chord location. In general, spanwise variations were found to be important. The upstream bow shock effect is non-linear in character. Comparisons to a two-dimensional, non-linear unsteady multi-blade row Navier-Stokes analysis at 50% span show a good agreement with the IGV unsteady surface pressure results and higher harmonic content. The results of the study indicate significant variations in the IGV unsteady loading caused by changes in axial spacing.

## NOMENCLATURE

c - chord length
p - pressure
t - time
x - distance along vane or blade

**Subscripts**
n - normalized
s - IGV inlet
1 - IGV upper surface
2 - IGV lower surface

## INTRODUCTION

Gas turbines are a vital energy source for both industrial and military applications with recent research focusing on identifying high cycle fatigue unsteady flow mechanisms. There is a constant need for an improved understanding of the flow physics through the various components. This greater understanding leads to the ability of manufacturers to achieve higher levels of performance and, in general, a more efficient system. As technology increases, there are continually increasing demands on gas turbine engines involving greater durability, reduced noise levels, reduced size and of course greater thrust. A jet engine consists of several distinct components; the inlet, compressor, combustor, turbine, and exit nozzle. A considerable portion of the recent research involves the unsteady interaction between adjacent blade rows in both the compressor and turbine sections.

The two principal types of blade row interaction are usually referred to as potential flow and wake interactions (Verdon, 1992). Potential flow interaction results from the variations in the velocity potential or pressure fields associated with the blades of a neighboring row and their effect upon the blades of a given row moving at a different rotational speed. This type of interaction is of serious concern when the axial spacing between adjacent blade rows is small or the flow Mach number is high. Wake interaction is the effect upon the flow through a downstream blade row of the vortical and entropic wakes shed by one or more upstream rows.

Recently, computational work has been initiated to develop non-linear, time-accurate, inviscid (Euler) and viscous (Navier-Stokes) solution techniques for unsteady flows through isolated and aerodynamically coupled blade rows (see Verdon, 1992 for a review). For coupled systems of rotating and stationary blade rows, the relative motions between adjacent rows give rise to unsteady aerodynamic excitations which can initiate blade vibrations, generate discrete-tone noise, and degrade aerodynamic efficiency. Two categories of numerical procedures have recently been developed for determining the effects of relative motion between adjacent blade rows. In the first category of numerical procedures, incoming wakes are specified at the inlet of isolated blade rows (Suddhoo et al., 1991). In these methods, the wakes are usually assumed to be parallel with uniform pressure and prescribed total enthalpy and/or velocity variations. In the second category of numerical analyses, both blade rows are modeled and the relative position of one blade row is varied to simulate blade motion (Giles, 1988, Rai, 1989, Rao and Delaney, 1990).

Some experimental investigations for compression systems have been made into vane/blade interactions. For compressors,

Presented at the International Gas Turbine & Aeroengine Congress & Exhibition
Indianapolis, Indiana — June 7–June 10, 1999

initial research was accomplished using low speed rigs (Kim and Fleeter, 1992) or annular cascades (Henderson and Fleeter, 1992). The low speed and large scale of these experimental rigs simplifies the measurements, but transonic flow phenomena, i.e., shock interaction, can not be modeled. Recently, high speed axial compressor research has been initiated. These facilities are beneficial for testing actual hardware components with research issues including miniature measurement techniques and data reduction methods. In particular, Johnston and Fleeter (1994, 1996, 1997) and Sanders and Fleeter (1998) have used a transonic compressor facility to investigate rotor wake phenomena, IGV/rotor potential fields, and rotor surface pressures. These research studies have provided an important initial step towards understanding the basic physics of the unsteady aerodynamic flow interactions in a compression system, but additional research is required.

In summary, little research has been directed at vane/blade interaction in a compressor section. Thus, relatively little is known about the unsteady IGV/blade interactions which occur within a compression system. Since these unsteady aerodynamic interactions can lead to high vibratory stresses, models must be developed to analyze vane/blade interaction. In addition, relevant experiments are needed to assess the validity of these models and direct future research efforts.

The objective of this research is to investigate and quantify the fundamental vane/blade interaction phenomena relevant to the upstream potential forcing function of a downstream rotor in a compression system. This is accomplished by performing a series of experiments in the Compressor Aero Research Lab (CARL), a high speed, highly loaded compression stage facility. IGV unsteady surface pressures are experimentally determined for different IGV/rotor spacings when operating at 105% speed. In addition, a non-linear unsteady multi-blade row computational (CFD) analysis is compared with the experimental data.

## RESEARCH FACILITY

**Compressor Aero Research Lab (CARL):** The experiments for this study were conducted in the Air Force Research Laboratory's Compressor Aero Research Lab facility at Wright-Patterson Air Force Base. The research compressor is a high speed, highly-loaded 1 1/2 stage compression system. The compressor facility consists of an open or closed loop (currently open) tunnel system with an upstream venturi flow meter to measure the mass flow rate. The compressor is driven by a 1490 kW electric motor with a variable speed range of 6,000 to 21,500 rpm.

The research compressor, Figure 1, was designed to simulate the second stage of a highly- loaded military core compressor. Wakes from a first stage are simulated by a upstream blade row. The primary intent for this research compressor is to investigate the influence of an upstream stage on the flow swallowing capability of a downstream transonic stage. Details on the compressor design are defined by Law (1989) and are summarized in Table 1.

To study the effect of different upstream stages, an IGV assembly is placed upstream of the rotor section. The IGVs were designed to create a wake consistent with a modern technology, highly loaded, low aspect ratio stage and maintain an axial inlet flow orientation. Therefore, they have a wide trailing edge as shown in Figure 2. They have a constant solidity (spacing to chord ratio) along the span and have no steady aerodynamic loading in order to achieve a uniform two-dimensional wake. In addition it is possible to vary the axial spacing between the IGVs and the rotor. Three different spacings are possible 12%, 26%, and 56% of the IGV chord from the IGV trailing edge to the rotor leading edge as shown in Figure 2. There are 24 IGVs in the upstream passage.

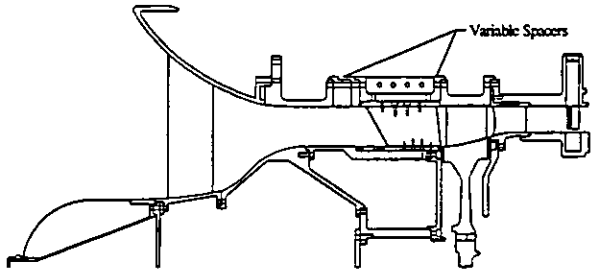


**Figure 1. Schematic of Flow Path**

| PARAMETER | ROTOR | STATOR |
|---|---|---|
| Number of Airfoils | 33 | 49 |
| Aspect Ratio - Average | 0.961 | 0.892 |
| Inlet Hub/Tip Ratio | 0.750 | 0.816 |
| Flow/Annulus Area, kg/sec | 18.14 | -- |
| Flow/Unit Area, kg/sed/m² | 0.738 | -- |
| Flow rate, kg/sec | 15.63 | -- |
| Tip Speed, Corrected m/sec | 341.4 | -- |
| $M_{REL}$ LE Hub | 0.963 | 0.820 |
| $M_{REL}$ LE Tip | 1.191 | 0.690 |
| PR Rotor | 1.880 | -- |
| $\eta_{iso}$ Rotor, % | 93.5 | -- |
| PR Stage | -- | 1.840 |
| $\eta_{iso}$ Stage, % | -- | 90.2 |
| D Factor Hub | 0.545 | 0.502 |
| D Factor Tip | 0.530 | 0.491 |
| LE Tip Dia., m | 0.4826 | 0.4826 |
| LE Hub Dia., m | 0.3620 | 0.3928 |
| TE Tip Dia., m | 0.4826 | 0.4826 |
| TE Hub Dia., m | 0.3872 | 0.4038 |

**Table 1. Compressor Design Parameters**

**IGV Surface Pressure Instrumentation:** The IGVs are instrumented with miniature Kulite pressure transducers. Figure 3 shows the locations of these pressure transducers. Two different blades are instrumented with 10 pressure transducers each. To investigate spanwise effects, two different spanwise locations are instrumented, 50% and 75% as shown measured from the hub. The blade surface is machined to allow the pressure transducers to be mounted flush. In order to protect the pressure sensor, a thin layer of RTV was placed over the diaphragm. Grooves for the lead wires were also machined to ensure no disturbance to the flow. The lead wires are bundled and fed out of the casing.

Two adjacent IGVs are instrumented giving data for one flow passage. Flow periodicity is assumed with one blade's data phase shifted to the other blade for analysis.

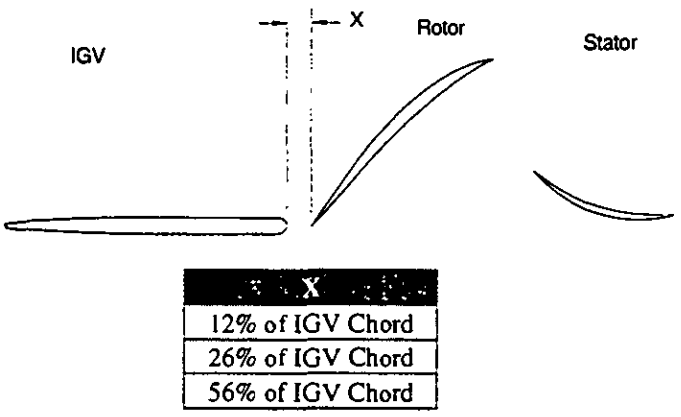


**Figure 2. Blade Profiles for Compressor at 50% IGV Span**

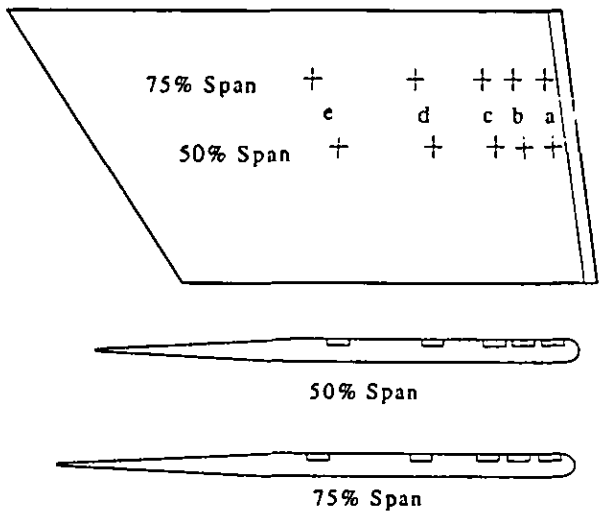


**Figure 3. Transducer Locations on IGV**

LQ-125 miniature pressure transducers from Kulite are used for the surface pressure measurements. The pressure transducers are manufactured directly on the blades with a 172.4 kPa maximum absolute pressure capability. The pressure sensing element is 0.1524 cm in diameter. It has an internally compensated temperature range of −1.1 to 54.4°C. The natural frequency of the pressure transducer is 300 kHz, giving a usable frequency range of 100 kHz.

Calibration of the transducers for sensitivity and offset was achieved in the following manner. Before installation of the instrumented wake generator, the transducers were subjected to variable pressures at a nominal temperature of 21.1°C and an elevated temperature of 43.3°C. The results of this study indicated for this range of temperature variation, the transducer sensitivity was 0.02% per °C. However, offset was influenced by temperature variation and the magnitude of the shift varied from a high of 0.2516 kPa/°C to a low of 0.0148 kPa/°C.

Based on this bench calibration, no special procedures were established to control sensitivity with inlet air temperature shifts. However, to control transducer offset variation, the transducers' amplifiers were re-balanced at atmospheric conditions for any inlet temperature shift of 1.4°C or greater.

From these procedures, offset and precision errors were established as ±0.41 kPa and ±0.28 kPa, respectively. In addition, a zero response data set was recorded. The data was then processed in the same manner as the actual test data. Therefore, this signal is representative of the actual static pressure uncertainty due to noise influences. The measured random uncertainty was a ±0.69 kPa fluctuation in static pressure. This value includes all errors due to random noise and temperature changes.

## COMPUTATIONAL ANALYSIS

A two-dimensional non-linear unsteady Euler/Navier-Stokes vane blade interaction model, VBI 2D, was developed by Rao and Delaney (1990), under sponsorship of the Air Force, for analysis of turbine configurations. The model analyzes the relative motion of adjacent blade rows by allowing one row to move with respect to the other. The VBI code was utilized to analyze the IGV/rotor interaction in the compression stage by modeling both the IGV and rotor. A brief overview of the VBI code will now be given.

**Grid Generation:** Two separate grids, an H grid and O grid, are generated for each blade row using VGRID. The two grids are then embedded to form a composite grid by a chimera scheme called PEGSUS (Benek et al., 1987). PEGSUS creates the appropriate hole boundaries and interpolation stencils needed for communication between the embedded grids. The embedding process gives better resolution of the boundary layer with the O grid, while eliminating cell skewness problems at the inlet and exit planes with the H grid. After the embedding process is completed, the PEGSUS results are read directly into the VBI code.

**Numerical Method:** The VBI code solves the Euler/Navier-Stokes equations using a explicit, second order accurate, Runge-Kutta scheme with higher-order dissipation in quasi-three-dimensional space. Residual smoothing is used to reduce the time required to reach a periodic quasi-steady solution. The Baldwin-Lomax (Baldwin and Lomax, 1978) algebraic eddy viscosity turbulence model is used for closure of the Navier-Stokes equations. While the transition from laminar to turbulent flow is performed using the Baldwin-Lomax model (Baldwin and Lomax, 1978).

**Boundary Conditions:** Non-reflective inflow and outflow boundary conditions are utilized for the H-grids with a reference plane method of characteristics scheme. For the O-grids, the reference planes are inherently non-parallel due to the fact that they are conforming to the airfoil shapes. It is then necessary for the VBI code to set the reference planes parallel to each other and perpendicular to the inflow boundary. This allows for the reference plane method of characteristics scheme to successfully be utilized at these boundary points. As the blade moves relative to the vane with the progression of a time step, the information from the previous time step is used to define the necessary vane outflow or blade inflow boundaries.

A phase-lagged technique is utilized for the blade-to-blade periodic boundary conditions. The computation is performed on one vane or blade from each row at a time. The solution fields for

adjacent vanes or blades are stored for the use in the phase-lagging procedure.

An overlapping of the H-grids at the vane outlet and blade inlet allows for information to be passed from one row to another. At least three cells must overlap for accurate information exchange. A bi-linear interpolation method is used to transfer the data from the IGV H-grid to the rotor H-grid to find the necessary boundary conditions.

## RESULTS

A series of experiments were performed to investigate the IGV unsteady surface pressure response due to the upstream traveling pressure field generated by the downstream rotor. The variable spacing feature of the experimental rig was used to study the effect that changing the axial spacing has on the unsteady IGV surface pressure measured at two spanwise locations. A computational study was then completed utilizing the VBI code with comparisons made to the experimental data.

**Experimental**: The experimental data was recorded on a 28 channel analog tape recorder with a flat response up to 80 kHz. The data was digitized off-line at an effective sample rate of 500 kHz by reducing the tape playback speed by one quarter and sampling at 125 kHz. Anti-aliasing was achieved using a Precision Filters TD6B Linear Phase Time Delay Filter. An effective cutoff frequency of 132 kHz was used for the data reduction. This gives a 1% attenuation of the signal at 77 kHz. The blade pass frequency is 7.8 kHz. Therefore, the first 10 blade pass harmonics are resolved without aliasing or attenuation. Data was digitized for a time record of 68 milliseconds as was dictated by storage limitations, which gives approximately 11 rotor revolutions. Ensemble averaging was performed on the data in order to average out any inconsistencies that may exist from one rotor blade to the next. The ensemble averaging was accomplished based on the rotor blade pass frequency, since the rotor has 33 blades, about 363 records were ensemble averaged. To assist in discussion of the results, the data is presented as two blade passages from the same averaged single passage record.

In order to analyze the effect that axial spacing has on the upstream IGV surface pressures, a 105% speed, peak efficiency operating point was used. The chosen operating point produces rotor relative Mach numbers of 1.22 and 1.15 for the 75% and 50% spans, respectively. A non-dimensionalized difference of the pressure values across the blade was determined from the measured absolute pressure data as defined by Equation 1.

$$p_n = \frac{p_1 - p_2}{p_S} \qquad (1)$$

The experimental results from all three axial spacings are shown on the same plot for comparison at each chordwise location. Averaged time resolved results from both spanwise locations are presented in Figures 4 and 6. Only four chordwise measurements are shown at 75% span due to a malfunctioning transducer at 50% chord.

**Axial Spacing Influences:** Figure 4a shows the 50% span, 95% chord location results. The 12% IGV chord axial spacing shows an unsteady normalized force of 0.39 (31.8 kPa) which is larger than the 0.20 (15.9 kPa) loading found at the 26% axial spacing. However, the 56% IGV chord axial spacing data shows a substantially smaller normalized force of 0.09 (7.25 kPa) on the blade, when compared to the closer spacings.

As shown in Figure 4a, there is a significant change in the unsteady loading with changes in axial spacing. These types of phenomena are important to engine designers, since typically no upstream unsteady loading is considered during the structural analysis of an engine. Therefore with the continued push for smaller and lighter engines, where axial spacings have decreased from approximately 50% to 25% of blade chord, these unsteady loads experienced by the upstream row must be consider in the engine design.

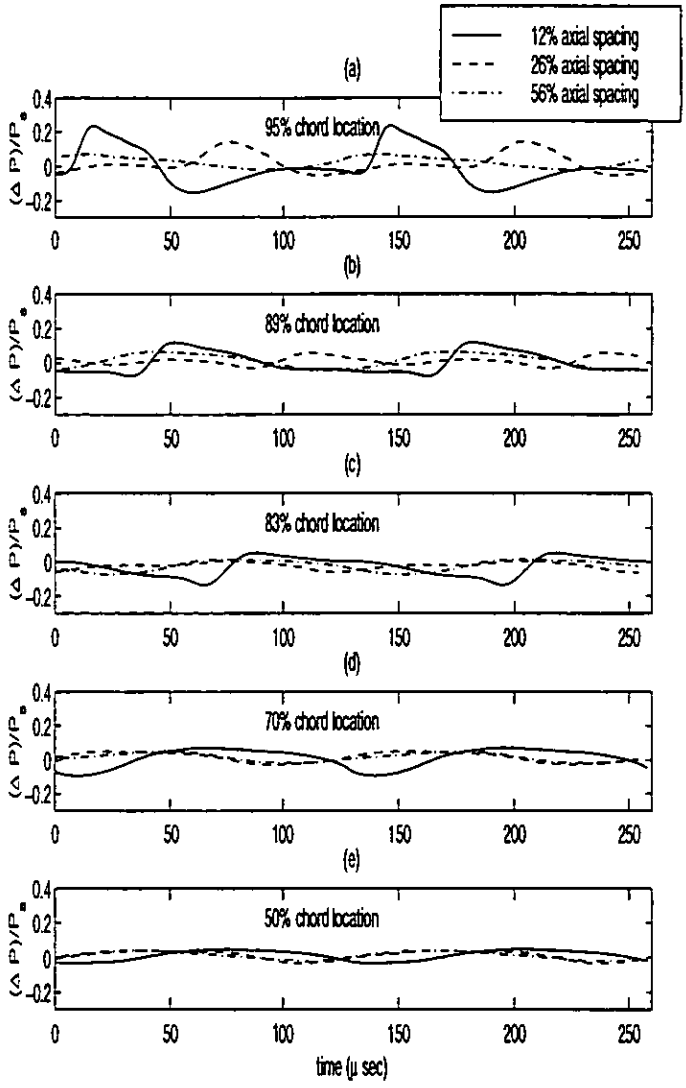


**Figure 4. Differenced Non-dimensionalized Pressure Time Traces for Three Axial Spacings: 50% Span**

Figure 4a also shows the phase shift, relative to the rotor leading edge, with changes in axial spacing. This figure clearly shows that the 12% IGV chord spacing leads the other axial spacings in phase. This is due to the fact that at the 12% spacing the rotor bow shock contacts the IGV surface earlier due to the decreased distance it has to travel before reaching the IGV trailing edge.

Figure 5 shows how (relative to a rotor blade position) the bow shock impinges on the 12% spaced IGV prior to the 26% and 56% spacings. The figure also demonstrates how the shock dissipates in the upstream direction from a sharp discontinuity in pressure resulting in high order harmonic loads on the close IGV, to a weak pressure wave resulting in a first order loading as the IGV spacing is increased.

In Figure 4b, the 89% chord, 50% span experimental data is given. Again, the 12% axial spacing unsteady pressure is dominant due to the close proximity between the rotor and the IGV trailing edge. As the spacing between the IGV and rotor is increased, a greater dissipation of the rotor bow shock occurs, decreasing the unsteady loading. The magnitude of the 12% IGV chord axial spacing data is 0.2 (15.9 kPa), which is a decrease from the 95% chord location due to the dissipation of the rotor bow shock moving upstream along the vane surface.

Figure 4c represents the 83% chord, 50% span location data. The 12% axial spacing data still shows an unsteady loading of 0.19 (15.4 kPa). The other spacings, 26% and 56%, show almost no net unsteady pressure response. Continuing to move upstream on the IGV surface, Figure 4d represents the 70% chord location experimental data. The 12% axial spacing still shows evidence of the upstream traveling forcing function with an unsteady pressure magnitude of 0.16 (13.1 kPa), while the other axial spacings show minimal interaction. Finally, Figure 4e shows a small first order unsteady pressure response at 50% chord and 50% span for all axial spacings, which is consistent with the trends shown in the previous results.

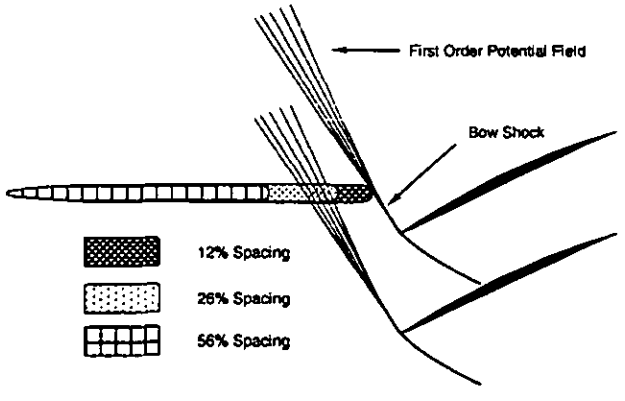


**Figure 5. IGV and Rotor Interaction**

The 50% span results reveal several trends. First, axial spacing variations have a significant effect on the upstream traveling unsteady pressure fluctuations generated by the downstream transonic rotor. Therefore unsteady loading on the upstream blade row should be included in the designing of gas turbines, especially as the axial spacing decreases. Secondly, we see that an overall decrease in the unsteady loading occurs as we move upstream along the IGV surface for each spacing and finally, that there is a change in phase with changes in axial spacing.

**Spanwise Variations:** In order to determine whether any radial variations affect the flow physics of the upstream traveling interaction, the 75% span experimental data is utilized. Figure 6 shows the 75% span location results for time traces of the unsteady delta pressure. At 95% chord, Figure 6a, the maximum unsteady

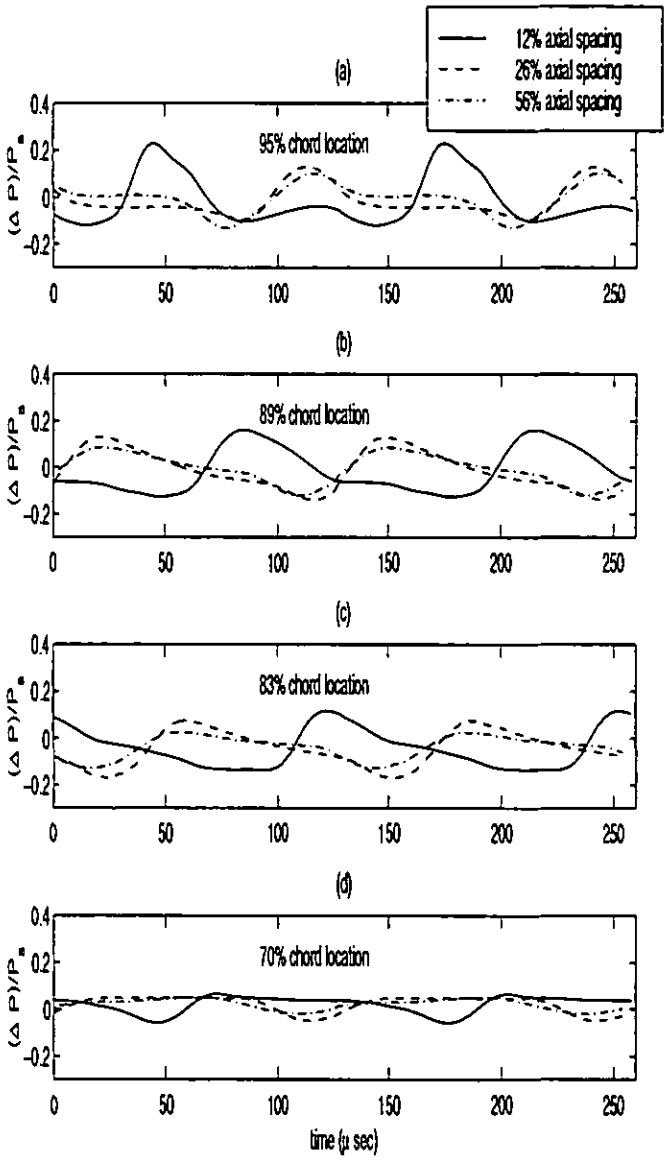


**Figure 6. Differenced Non-dimensionalized Pressure Time Traces for Three Axial Spacings: 75% Span**

loading is 0.35 (28.4 kPa) at 12% spacing which is slightly smaller than the loading at 50% span, Figure 4a. However, the pressure fluctuation at 56% spacing for 75% span is significantly greater than the loading at 50% span, 0.23 (18.9 kPa) to 0.09 (7.25 kPa), respectively. Figure 6a shows the same phase shift with respect to axial spacing as the 50% span results.

In Figure 6b, the 89% chord location results show a decrease in magnitude to 0.29 or 23.3 kPa for the 12% axial spacing. The bow shock interaction is still evident at this further upstream location. Compared to the 50% span results the unsteady loading is significantly greater for all three axial spacings. For instance, at the 89% chord and 12% axial spacing, the unsteady magnitude is 0.091 (7.39 kPa) greater at 75% span than 50% span. This trend is consistent with the increased relative Mach number at 75% span resulting in a stronger rotor bow shock. Therefore, the overall dissipation of the shock with axial spacing is less at 75% span resulting in larger unsteady loads, which are important in engine design.

Figure 6c shows the 83% chord data, where again all three spacings show significant unsteady response with a slightly decrease magnitude. The 12% axial spacing unsteady pressure magnitude is 0.25 or 20.5 kPa, which is nearly 50% of the loading at the 95% chord location, Figure 6a. Finally, the 70% chord 75% span location results, Figure 6d, show that only the 12% axial spacing exhibits any unsteady loading.

In summary all of the trends found at 50% span were also evident in the 75% span results. However, spanwise variations in the compressor stage are evident as shown by comparison of the results shown in Figures 4 and 6. In general, the unsteady pressure loading is greater at 75% span than at 50% span, while dissipation of the unsteady loading with axial spacing was less at 75% span than at 50%. Therefore, the upstream propagating unsteady pressure fluctuation persists further upstream at the larger span location. This could be attributed to the higher relative Mach number at the 75% span.

**Chordwise Variations:** Figure 7, shows the influence of absolute upstream position on the measured blade surface peak-to-peak dynamic loading for both spanwise locations and each IGV axial spacing. Figure 7a at 50% span suggests that the peak-to-peak pressure loading tends to collapse regardless of IGV axial spacing for locations greater than 100% rotor chord upstream of the rotor, while for 75% span (Figure 7b) no evidence of this phenomena can been seen through 150% rotor chord. Since the peak-to-peak pressure loading does not collapse to one value at a given absolute axial location, the IGV cannot be considered a passive device in the flow field, with no influence on the rotor upstream potential forces. Instead the figure shows that for both 50 and 75% span the IGV's interact with the rotor potential field and their axial spacing influences the measured peak-to-peak pressure forces. This experiment demonstrates the importance, in this case, of modeling the IGV-rotor interaction accurately, rather than assuming a simple exponential decay of the rotor potential field.

**Harmonic Content:** Figure 8 demonstrates the higher-order harmonic content for all three axial spacing data sets through a Fast Fourier Transform analysis. The 105% speed, peak efficiency operating point data was used for the analysis at the 95% chord and 75% span location. The blade pass frequency is not the dominant response at this location. The second harmonic at 12% axial spacing is the same magnitude as the first, while at 26% and 56% axial spacing, the second harmonic is approximately 90% of the first harmonic. In addition, the third harmonic is nearly a third of the first at both 12% and 26% axial spacing, with the 56% spacing magnitude being negligible. It should be noted that the slight shift in frequency, with axial spacing, is due to changes in the mechanical wheel speed since only the mass flow was matched for each configuration. Figure 8 clearly shows the importance of the higher harmonic responses in capturing the vane forced response. Therefore, this result demonstrates the necessity to consider these harmonics during a CFD analysis.

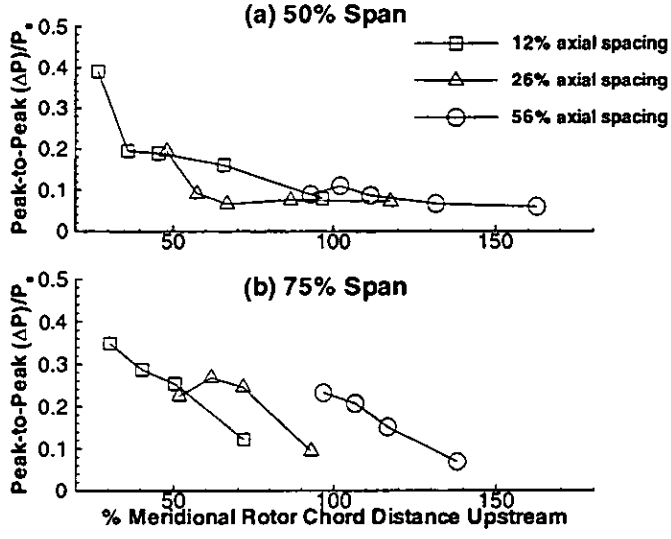


**Figure 7. Chordwise Variation in Peak Pressure Loading**

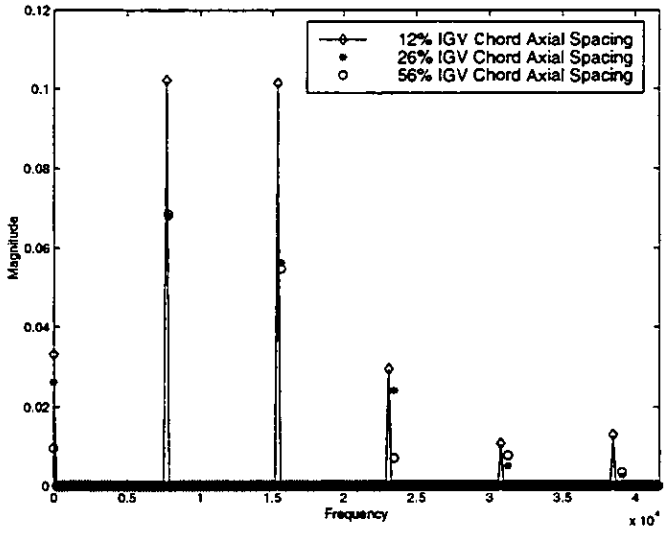


**Figure 8. FFT of Peak Efficiency: 95% Chord Experimental Data**

**Computational:** Computational results will now be shown for the 105% speed, peak efficiency operating point. An analysis for two axial spacings was performed using the 12% and 26% IGV chord locations at 50% span. When performing the computational runs, it was first necessary to complete an initial steady state analysis using the VBI code. The steady computation was accomplished using the VBI solver with no communication between the two blade rows. During the initial run the rotor was in motion but the IGV row was isolated removing any possible affects created by the rotor. The steady analysis was then used as an initial flow field for the unsteady analysis decreasing some of the initial unsteady transients, therefore an initial 3500 steady "time" steps are used for all of the computational results. A grid independence check was done for the CFD analysis, resulting in a 281x27 and 351x27 O-grid and a 273x93 and 293x93 H-grid for the IGV and rotor, respectively at 12% axial spacing. The same O-grids with 288x93 and 306x93 H-grids for the IGV and rotor, respectively, were used for the 26% axial spacing. The number of times steps per rotor blade pass for each run was 3840. A total of 100,000 time steps were needed for each run to reach a unsteady converged solution. Figure 9 represents a pressure time history for one node of the flow field for the 12% axial spacing. A total of 25 rotor blade passes were analyzed to reach the nearly periodic solution shown in Figure 9. For the quasi-three-dimensional effects, a 30% stream tube contraction through the rotor is input. Finally, in modeling the current experimental configuration, 24 IGVs and 33 rotor blades, it was possible to reduce the required blade row numbers down to 8 IGVs and 11 blades due to periodicity. A phase-lagged boundary condition was then utilized making it possible to perform the computations on one vane or blade of each row at a time by using stored data from previous blade positions.

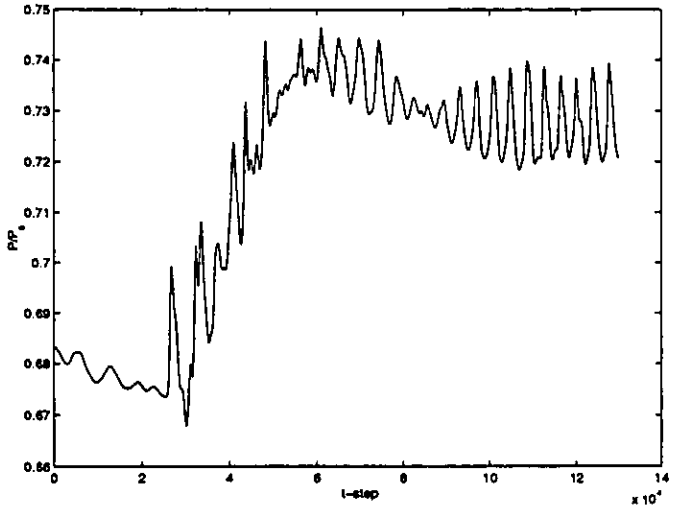


**Figure 9. Pressure Time History for Convergence Check**

**12% IGV Chord Axial Spacing Analysis:** A comparison with experimental data of the local blade loading on the IGVs is shown in Figure 10. The computational results shown are for the last two blade passes of the 25 total. As can be seen in the figure, the computed interaction decreases from the trailing edge to the leading edge.

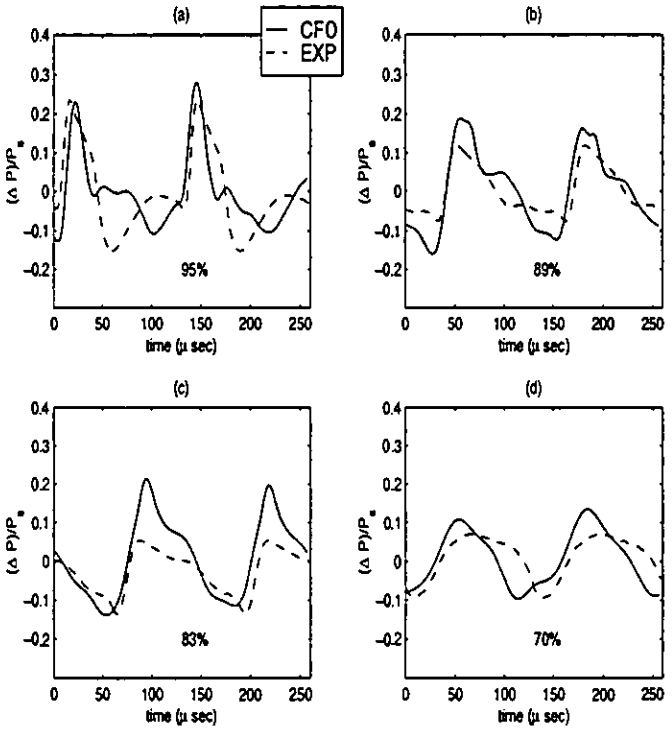


**Figure 10. Computational and Experimental Pressure Data: 50% Span - 12% IGV Chord Axial Spacing**

At the 95% chord location, Figure 10a, both the experiment and computations show the steep pressure rise due to the bow shock, with the CFD results showing good agreement in magnitude and phase. At the 89% chord location, Figure 10b, the shock structure is still the dominating physical phenomenon. The computational analysis slightly over-predicts the unsteady magnitude response with the phase in excellent agreement. At 83% chord, Figure 10c, the experimental results show that the shock has dissipated, while the computational results remain relatively unchanged. This over prediction is conceivably due to inaccurate modeling of the viscous dissipation effects present in the experiment. At the 70% chord location, the CFD results show continued general agreement with the experimental data in regards to magnitude and phase with decreased response.

The computational results at the 12% IGV chord axial spacing reveal several trends. First, the computational model predicted the magnitude and phase of the unsteady pressure on the IGV surface very well for the close spacing. In addition, the non-linear model predicted the strong bow shock interaction at the trailing edge quite accurately.

**26% IGV Chord Axial Spacing Analysis:** For the 26% axial spacing the final two blade passes are compared with the experimental data, Figure 11. For this spacing, the computational results over predict the overall pressure magnitudes at each chordwise position. Figure 11a, shows the 95% chord comparison. The computational results do not show good periodicity at this location, while slightly over predicting the unsteady pressure magnitude. The 89% results, Figure 11b, show reasonable phase agreement but the unsteady pressure magnitude is considerably larger than in the experimental data. There is a lack of phase agreement for the 83% and 70% chord locations, Figures 11c and 11d. The magnitudes for these chordwise locations are considerably over predicted as well. The CFD model does tend to under predict the upstream propagating unsteady pressure dissipation.

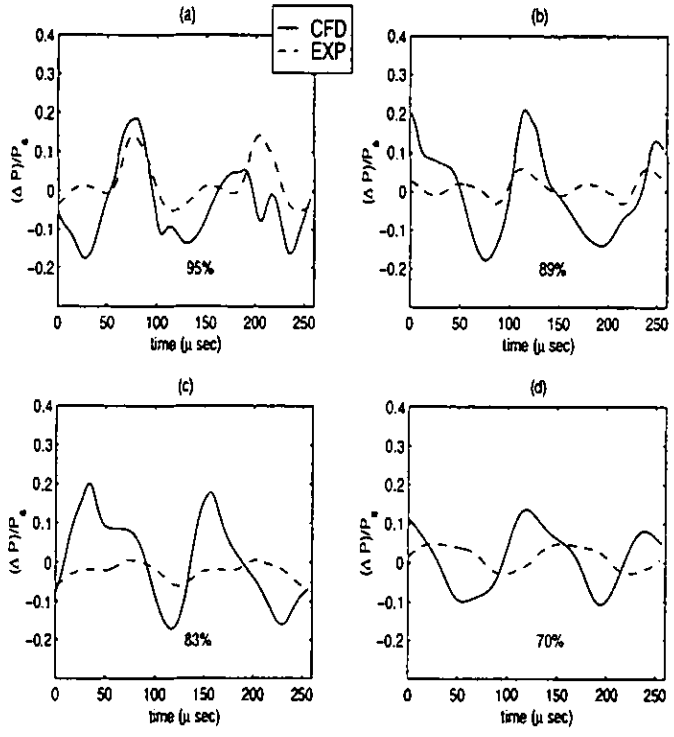


**Figure 11. Computational and Experimental Pressure Data: 50% Span - 26% IGV Chord Axial Spacing**

**Harmonic Content:** Figure 12 shows the frequency response of both the computational and experimental data for the 12% IGV axial spacing and 95% chord location. Good agreement is shown in terms of the harmonic content except for the second harmonic, which is under predicted. The experimental results show the importance of the higher harmonic contributions of the rotor bow shock on the unsteady loading and the non-linear computational results show good agreement. For the 26% IGV axial spacing, Figure 13, the harmonic content of the experimental results are considerably reduced compared to the 12% results, but the computational results do not predict this larger harmonic decay. The CFD results significantly over predict the harmonic magnitudes for the fourth and fifth harmonics when compared to the fourth and fifth harmonic predictions for the 12% axial spacing, Figure 12.

The unsteady pressure response at the blade pass frequency is the largest, but the magnitudes of the higher harmonics are important as well, thereby, creating a necessity to perform either a non-linear analysis or a linearized analysis through superposition of the higher harmonics. The non-linear Navier-Stokes analysis predicts the frequency content well, but care should be taken, because the viscous dissipation may be under predicted resulting in a prediction of too large of an unsteady loading.

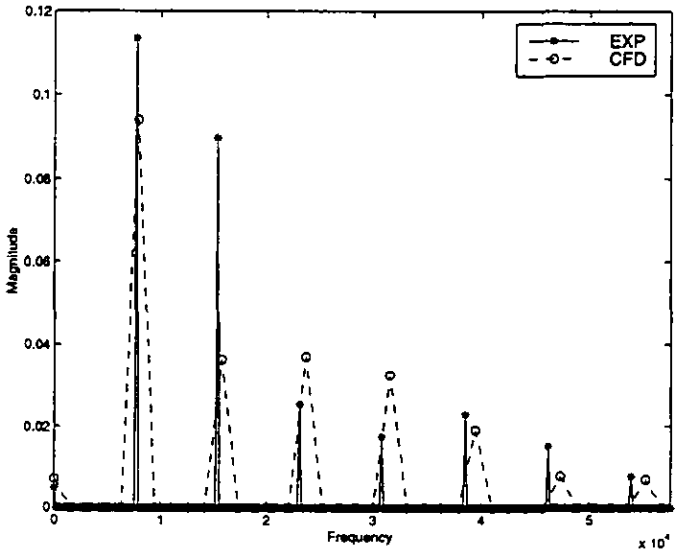


**Figure 12. Frequency Response: 12% Axial Spacing 95% Chord**

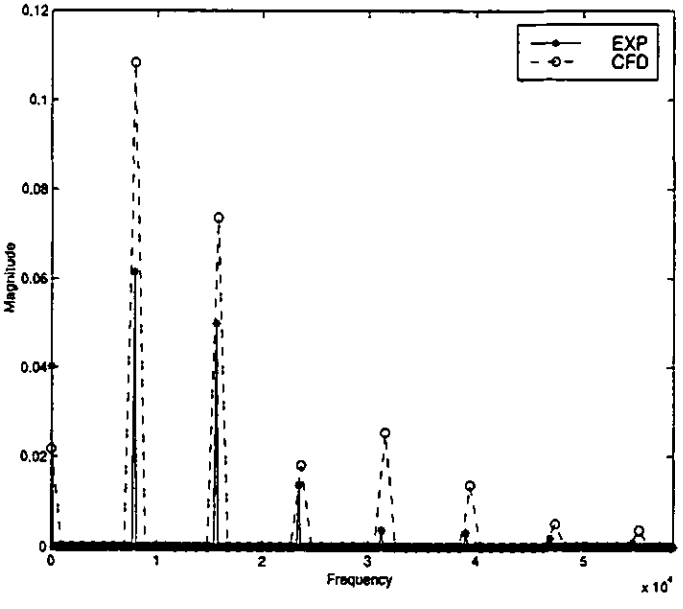


**Figure 13. Frequency Response: 26% Axial Spacing 95% Chord**

## SUMMARY AND CONCLUSIONS

A series of experiments was performed to investigate the unsteady upstream traveling forcing function from a high speed, highly loaded compressor rotor. These experiments were performed for several different axial spacing between the IGV and rotor rows, as well as at different spanwise locations. The IGV unsteady surface pressures were measured to determine the forced response. The experimental configuration was computationally modeled with a non-linear unsteady vane/blade interaction two-dimensional viscous code for comparison.

This investigation reveals several significant fundamental flow physics phenomena: (1) upstream traveling unsteady pressure fluctuations are significant; (2) the rotor bow shock dominates the pressure variations; (3) changes in axial spacing effects the magnitude and character of the unsteady pressure loading; (4) a non-linear CFD model showed a favorable comparison in terms of unsteady pressure magnitude, phase and harmonic content for the 12% axial spacing study, but the viscous dissipation of the unsteady effects were under predicted for the 26% results; (5) the higher harmonic content of the unsteady pressure variations are significant in understanding the transonic compressor flow physics.

## ACKNOWLEDGMENTS

The authors would like to thank Dr. Herb Law, Mr. Steve Gorrell, Mr. Ron Berger, Mr. Bob Wirrig, Mr. Bill Uhlman and Mr. Terry Norris at CARL for their excellent support in obtaining the experimental data. The data quality is a true testament to their dedication towards excellence. The authors would also like to thank Dr. Rolf Sondergaard and Mr. Charles Stevens from AFRL/PRTT for help with the computational results. In addition, the authors acknowledge the financial support of the Dayton Area Graduate Studies Institute (DAGSI), a Ohio Board of Regents Research Challenge Grant, the AFOSR summer research program and a AFOSR extension grant. Finally, this work was supported in part by a grant of HPC time from the DoD ASC MSRC at Wright Patterson Air Force Base.

## REFERENCES

Baldwin, B. and Lomax, H., 1978, "Thin Layer Approximation and Algebraic Model for Separated Turbulent Flows," *AIAA Paper No. 78-257.*

Benek, J.A., Donegan, T.L. and Suhs, N.E., 1987, "Extended Chimera Grid Embedding Scheme with Application to Viscous Flows," *AIAA Paper No. 87-1126-CP.*

Giles, M.B., 1988, "Stator/Rotor Interaction a Transonic Turbine," *AIAA Paper No. 88-3093.*

Henderson, G.H. and Fleeter, S., 1992, "Airfoil Wake and Linear Theory Gust Response Including Sub and Super-resonant Flow Conditions," *AIAA Paper No. 92-3074.*

Johnston, R.T., Feiereisen, J.M. and Fleeter, S., 1994, "Rotor Wake and Potential Forcing Functions, Including Blade Row Interactions," *AIAA Paper No. 94-2975.*

Johnston, R.T. and Fleeter, S., 1996, "Time-Resolved Variations of an IGV Flow Field in the Presence of a Rotor Potential Field," *AIAA Paper No. 96-2670.*

Johnston, R.T. and Fleeter, S., 1997, "Rotor Blade Pressure Measurement in a High Speed Axial Compressor Using Pressure and Temperature Sensitive Paints," *AIAA Paper No. 97-0162*

Kim, K.H. and Fleeter, S., 1992, "Compressor Blade Row Unsteady Aerodynamic Response to Attached and Separated Flow Forcing Functions," *AIAA Paper No. 92-0147.*

Law, C.H., 1989, "Two Axial Compressor Designs for a Stage Matching Investigation," AFWAL-TR-89-2005.

Rai, Man Mohan, 1989, "Three-Dimensional Navier-Stokes Simulations of Turbine Rotor-Stator Interaction; Part I-Methodology," *Journal of Propulsion*, Vol. 5, No. 3, pp. 305-311.

Rao, K.V. and Delaney, R., 1990, "Investigation of Unsteady Flow Through Transonic Turbine Stage; Part I: Analysis," *AIAA Paper No. 90-2408.*

Sanders, A. and Fleeter, S., 1998, "An Experimental Investigation of IGV-Rotor Interaction in a Transonic Axial-Flow Compressor," *AIAA Paper No. 98-3291.*

Suddhoo, A., Giles, M.B. and Stow, P., 1991, "Simulation of Inviscid Blade Row Interaction Using a Linear and a Non-Linear Method," *AIAA Paper No. 91-7049.*

Verdon, J.M., 1992, "Unsteady Aerodynamic Methods for Turbomachinery Aeroelastic and Aeroacoustic Applications," *AIAA Paper No. 92-0011*